

The Beginning of the End: *Hubble Space Telescope* Images of Seyfert's Sextet

Christopher Palma, Stephanie G. Zonak, Sally D. Hunsberger, Jane C. Charlton, Sarah C. Gallagher, Patrick R. Durrell

Department of Astronomy & Astrophysics, Pennsylvania State University

Email: cpalma@astro.psu.edu, szonak@astro.psu.edu, sdh@astro.psu.edu, charlton@astro.psu.edu, gallsc@astro.psu.edu, pdurrell@astro.psu.edu

and

Jayanne English

University of Manitoba

Email: Jayanne_English@umanitoba.ca

ABSTRACT

Hubble Space Telescope Wide Field Planetary Camera 2 images of Hickson Compact Group 79, Seyfert's Sextet, are presented. Both point sources and extended sources detected on the three WF chips were photometered in four filters: F336W, F439W, F555W, and F814W. Unlike other HCGs that have been imaged with *HST*, there do not appear to be any candidate young star clusters among the detected point sources. The majority of the point sources that may be star clusters associated with the Sextet have red colors consistent with stellar populations older than 1 Gyr. A similar conclusion is drawn with regard to the extended sources. The majority of these appear to be background galaxies, but a few candidate dwarf galaxies are identified as potentially associated with Seyfert's Sextet. However, no blue, star forming objects similar to the tidal dwarf galaxy candidates identified in other HCGs are found among the extended objects identified in this study. A redshift for one dwarf galaxy candidate was measured from a spectrum obtained with the Hobby-Eberly Telescope, and this object was found to have a redshift similar to NGC6027e, the discordant spiral formerly identified as a member of this compact group. The *HST* observations presented here and previous radio observations of the neutral gas content of this group suggest that the interactions that have taken place in the Sextet only redistributed the stars from the member galaxies within the group. We speculate that future interactions may be strong enough to strip the gas from NGC6027d and trigger star cluster formation.

Subject headings: galaxies: individual (NGC6207) — galaxies: interactions — galaxies: star clusters

1. Introduction

Compact groups of galaxies are found at the extreme end of the distribution of galaxy surface densities; by definition, compact groups consist of four or more isolated galaxies found within a small area on the sky. Using the Hickson (1982) compact group selection criteria, the surface densities of galaxies in compact groups are similar to or larger than those found in the centers of massive galaxy clusters. A radial velocity survey of the 100 Hickson compact groups (HCGs; Hickson et al. 1992) has verified that the majority of these HCGs are physical associations of 3 or more galaxies with a median velocity dispersion of 200 km sec^{-1} . One expects that in such dense groups with small velocity dispersions that interactions and mergers among the members are inevitable.

As expected, the morphologies of the galaxies in compact groups often show evidence of tidal interaction. Galaxy mergers are complicated phenomena, and it is difficult to disentangle the past histories of the merging galaxies, even in isolated, merging pairs. In compact groups there is often evidence for multiple interactions (e.g., Hickson 1982), so unravelling the history of these systems is even more of a challenge. Fortunately, star formation is a useful tool for dating some of the discrete events in the interaction history of a galaxy merger.

Relying on *Hubble Space Telescope* (*HST*) images, a growing number of studies have found evidence for compact star cluster formation in systems of interacting galaxies or merger remnants (Holtzman et al. 1992; Whitmore et al. 1993; O’Connell et al. 1995; Schweizer et al. 1996; Miller et al. 1997; Zepf et al. 1999; Johnson & Conti 2000; Gallagher et al. 2001). Using stellar population synthesis models, the ages of the observed young star clusters can be estimated from their photometric colors. In cases where discrete populations of young clusters are found in different regions of an interaction or merger remnant, variations among the ages of the clusters can be used to date events in the merger history. For example, Whitmore et al. (1999) identified four distinct populations of young star clusters in the “Antennae” (NGC 4039/39), and used the ages of these populations to infer some of the evolutionary history of this system. Gallagher et al. (2001) have identified a number of compact clusters in HCG 92, Stephan’s Quintet. This system is more complicated than the Antennae, but the star cluster ages have been used to identify distinct epochs of cluster formation and to date some of the interaction events.

Star formation in interacting galaxies is not necessarily limited to compact cluster formation; there is also observational evidence for the formation of extended, dwarf galaxy-sized objects in the tidal debris of a number of systems (e.g., Mirabel, Lutz, & Maza 1991; Mirabel, Dottori, & Lutz 1992; Hibbard et al. 1994; Deeg et al. 1998; Duc & Mirabel 1998; Duc et al. 2000; Mendes de Oliveira et al. 2001). Hunsberger et al. (1996, 1998) have performed a statistical analysis of a large sample of HCGs and found evidence that tidal dwarf galaxy formation in compact groups may be common. Numerical simulations suggest that dwarf galaxy formation in tidal tails is possible (Barnes & Hernquist 1992; Elmegreen et al. 1993); however, it is unclear whether the observationally identified “tidal dwarf galaxies” (TDGs) will evolve into the bound entities seen in the simulations.

Recently, a few groups have presented dynamical analyses of several TDGs (Duc et al. 2000; Mendes de Oliveira et al. 2001; Hibbard et al. 2001) in order to assess the likelihood that these objects will remain bound, but the results remain ambiguous.

HST imaging of HCGs is useful for addressing both the interaction history of a compact group as well as the presence and nature of any putative TDGs. In this paper, we present Wide Field Planetary Camera 2 (WFPC2) observations of Hickson Compact Group 79, Seyfert’s Sextet, taken in the *U*, *B*, *V*, and *I* (F336W, F439W, F555W, and F814W) filters. In Sections 2.2–2.4, the compact clusters in the group are identified and their ages estimated from stellar population models. In Sections 2.5–2.6, we present the extended objects in the field and discuss their nature. Section 3 discusses a spectroscopic follow-up observation of one candidate dwarf galaxy associated with the Sextet. Finally, in Section 4, we compare the population of compact clusters and dwarf galaxies in Seyfert’s Sextet to those found in the recent *HST* studies of HCG 92 (Stephan’s Quintet; Gallagher et al. 2001) and HCG 31 (Johnson & Conti 2000).

2. Observations of Seyfert’s Sextet

Seyfert (1948, 1951) was the first to identify and study this “unusually densely crowded group of six galaxies” from photographic plates taken with the Harvard Schmidt telescope. While the second article refers to six galaxies and does name the group a sextet, Seyfert (1951) mentions that Baade’s observations of the group show that the object labeled “NGC6027e”¹ is “not a separate galaxy but a tidally distorted part of NGC6027.” Seyfert (1951) goes on to say that “If this is actually the case, we have a very extraordinary filament which not only has a perceptible condensation but a filament which is nearly twice as large as the parent spiral.” Based on the morphological differences between the two late-type spirals and the tidally distorted early-type spirals, Seyfert (1951) considered two possibilities: (1) the Sextet is truly comprised of three physically associated early-type galaxies, two background spirals, and one bright tidal tail, or (2) it is a physically associated group of six galaxies.

Seyfert’s Sextet fits the criteria for inclusion in the Hickson compact group catalogue (Hickson 1982). It is the most compact of the HCGs (Hickson 1997), with a median galaxy separation of $9.1h_{75}^{-1}$ kpc (we adopt $H_0 = 75 \text{ km s}^{-1} \text{ Mpc}^{-1}$ throughout this paper). The group is now known to consist of four galaxies with accordant redshifts, one bright tidal tail, and a fifth galaxy at a redshift much larger than the group median redshift (Hickson et al. 1992). Using the mean redshift of the accordant galaxies, $z = 0.0145$ (Hickson et al. 1992), the distance to the Sextet is $57.5h^{-1}$ Mpc and the distance modulus is 33.8 magnitudes. A summary of the global properties of Seyfert’s Sextet is given in Table 1. In Figure 1, we present an image of Seyfert’s Sextet from the second

¹Note that Seyfert’s designations for the individual galaxies, NGC6027 and NGC6027a-e, are not the same as the commonly adopted, modern designations for the galaxies. Throughout this article, we use the designations adopted later by Hickson (1982). The galaxies in the Sextet are labeled in the image presented as Figure 1.

generation red Digitized Sky Survey² that includes labels for the individual member galaxies using the scheme of Hickson (1982).

2.1. *HST* Observations

The WFPC2 instrument on the *Hubble Space Telescope* was used to observe Seyfert’s Sextet in 2000 June (program ID 8717, Hunsberger PI). The observations were planned in such a way as to place the Sextet galaxies on the three Wide Field chips. Because of the placement of the galaxies of interest on the three WF chips, and since additional read noise in the PC data raises the detection threshold for point sources on this chip compared to the WF chips, the Planetary Camera data were not included in this study. The total exposure time in each filter was broken up into four cosmic ray-split exposures. One dithering offset of ~ 2.5 pixels in the x and y directions was introduced so that two of the four subexposures are at one dither location and the other two subexposures are at another. The exposure times were 4×500 seconds in F814W and F555W and 4×1300 seconds in F439W and F336W. The gain was set to $7\ e^-/\text{ADU}$ during these exposures.

In order to use the latest *HST* calibration, the data were recalibrated with the “best” reference files available from the *HST* archive in 2002 January. Known hot pixels were removed from the images using the IRAF³ STSDAS task WARMPIX. After hot pixel removal, the two images at each dither position in each filter were averaged together with GCOMBINE and then further cleaned of cosmic rays with the IRAF task COSMICRAYS. Identification and photometry of point sources (see §2.2) were done individually on each of the images of the two dither locations and the results subsequently averaged. The choice to analyze each dither location separately was made because the detection of extremely faint sources and the study of the sizes of these objects are not the focus of this paper. Using the IRAF tasks GEOMAP and GEOTRAN to solve for the transformation between the two dither locations, a final, combined image in each filter that retains the original pixel scale was created. Identification and photometry of the extended sources in the field were done on the final, combined image (see §2.5).

Also, a color image of Seyfert’s Sextet (Figure 2) was created by combining the black and white data collected through the 4 filters. The intensities were first clipped and scaled to bring

²The Digitized Sky Survey was produced at the Space Telescope Science Institute under U.S. Government grant NAG W-2166. The images of these surveys are based on photographic data obtained using the Oschin Schmidt Telescope on Palomar Mountain and the UK Schmidt Telescope. The plates were processed into the present compressed digital form with the permission of these institutions. The Second Palomar Observatory Sky Survey (POSS-II) was made by the California Institute of Technology with funds from the National Science Foundation, the National Aeronautics and Space Administration, the National Geographic Society, the Sloan Foundation, the Samuel Oschin Foundation, and the Eastman Kodak Corporation.

³IRAF is distributed by the National Optical Astronomy Observatories, which is operated by the Association of Universities for Research in Astronomy, Inc., under cooperative agreement with the National Science Foundation.

out faint emission. (KARMA’s Kview task was employed for this step but the remainder of the manipulations were accomplished using GIMP.) Each filter’s scaled image was then assigned a color that approximated the peak wavelength of that filter: F336W was colored reddish-violet, F439W blue, F555W yellowish-green, and F814W red. These colour images were combined using the “screen” algorithm in GIMP. The contrast of the combined image was adjusted to produce a neutral, dark background and emphasize particular features. It is the inclusion of the ultraviolet filter that causes the disk of the central spiral galaxy, as well as the central regions of the edge-on spiral, to be rendered more pink than they would be if strictly optical filters were used.

2.2. Point Source Detection

The method used for point source detection follows very closely the technique used by Gallagher et al. (2001). A brief summary of this method is presented here: Each dither location in each filter was initially searched for point sources using the DAOFIND task within IRAF’s implementation of DAOPHOT (Stetson 1987). The detection threshold was set very low in order to find potential sources in regions of higher than average background (e.g., in the faint tidal tail). In order to remove some spurious detections, only those objects detected at the same location in both dither images were retained. Initial aperture photometry was performed on this large number of objects (thousands per WF chip), and all objects with $S/N < 3.0$ at either or both dither locations were thrown out.

Although this process serves to eliminate most of the spurious sources, a number of objects remain in the catalogue that can be eliminated as potential compact star clusters associated with Seyfert’s Sextet. Adopting the mean group redshift as a distance measure, the Sextet is $\sim 58 h_{75}^{-1}$ Mpc from Earth, and at this distance, one pixel is $\sim 27 h_{75}^{-1}$ pc. Typical Galactic globular clusters have $r << 27$ pc (Harris 1996), and even large, young clusters seen in the Antennae have effective radii (the radius enclosing half of the light, seen in projection) of $r_{eff} < 15$ pc, which leads us to expect that compact clusters in the Sextet will be unresolved. Thus, we can clean the catalogue further by eliminating all resolved sources.

Resolved sources were removed from the catalogue using the same set of tests used by Gallagher et al. (2001) (which are derived from those in Miller et al. 1997). Specifically, at each dither location, every potential point source was photometered with an aperture radius of 0.5 pixels and a second time with an aperture radius of 3.0 pixels. The difference in the V magnitude between the two apertures, $\Delta V_{0.5-3.0}$ was calculated, and all objects with $\Delta V_{0.5-3.0} < 0.5$ (likely cosmic rays or other hot pixels) or $\Delta V_{0.5-3.0} > 2.5$ (resolved sources) in either pointing were flagged. Also, using the IRAF task RADPROF, fifth order cubic splines were fit to the radial profiles of each potential point source. In all four filters, the mean FWHM for the likely point sources is 1.0 – 1.1 pixels, however the peak of the four distributions are near 0.9 pixels, with a non-Gaussian tail to higher values. To separate real point sources from resolved sources, we chose to flag those objects with FWHM > 2.0 pixels, also. Each object was thus tested four times: once with the $\Delta V_{0.5-3.0}$ test

and once with the FWHM test at each dither location. Any object with two or more flags was removed from the catalogue of point sources.

The final catalogues did contain some sources that passed all algorithmic tests, but could still be easily ruled out as potential compact star clusters. These included bright, foreground, Galactic stars, the unresolved nuclei of a few background galaxies, and H II regions in the disk of the background galaxy in the Sextet (NGC 6027e). The foreground stars and galactic nuclei are easily distinguishable from the candidate star clusters. Although the H II regions in NGC 6027e are blue point sources that might be mistaken for star cluster candidates, they are all aligned with the prominent spiral arms in this disk galaxy, so we are confident that they are unlikely to be point sources associated with Seyfert’s Sextet. We removed by hand these three types of contaminating objects from the catalogue. In the end, we were left with a total of 188 star cluster candidates (see Figure 3 for a finding chart) detected in at least one filter. Very few objects were detected in the two blue filters, F439W and F336W; we discuss this further in §2.4.

2.2.1. Sub-pixel Dithering

The exposures of Seyfert’s Sextet were taken at two dither locations and can be combined in order to enhance the angular resolution using the “DRIZZLE” software developed by Fruchter & Hook (2002). Since the cluster population of Seyfert’s Sextet should be unresolved even in drizzled images, we chose to apply our cluster detection algorithm to the raw, undrizzled images rather than to drizzled images. However, we did combine the F439W and F555W images of the WF2 chip with the drizzle software in order to test the differences in cluster detection on drizzled and undrizzled images. Drizzle was run with the parameters $pixfrac = 1.0$ and $scale = 0.5$, which is equivalent to the “shift and add” technique, and the resulting images have a pixel scale twice as fine as that of the input images.

We used an identical cluster detection algorithm to the one described above: The objects detected by DAOFIND in the F439W and F555W drizzled and undrizzled images were pruned first by signal-to-noise and then were pruned further using the FWHM and $\Delta V_{0.5-3.0}$ (the aperture sizes were doubled to 1.0 pix and 6.0 pix for the drizzled image) tests discussed in detail in the previous section. The most significant cut is the signal to noise cut; since the threshold used in DAOFIND is so low, many of the objects detected have $S/N < 2.5$. Furthermore, there are significant (at the $\sim 10\%$ level) differences in S/N between the objects in the drizzled image and in the undrizzled image. This is especially true of objects found in regions where the background is variable, such as within the bright isophotes of NGC6027a and NGC6027d. After applying our signal to noise criterion, a number of (likely spurious) objects within the bright isophotes of these two galaxies remain in the catalogue created from the undrizzled image. However, in comparison, many of these get removed from the catalogue created from the drizzled image.

The second criterion used to flag objects for removal from our point source catalogues are the

“structure” parameters – FWHM and the concentration or $\Delta V_{0.5-3.0}$. What we find is that objects that have $0.5 < \Delta V_{0.5-3.0} < 2.5$ lie in a narrow range of FWHM, indicating that they are likely to be point sources. Almost every object within this window of concentration parameter have FWHM < 2.0 pixels in the undrizzled image and FWHM < 4.0 pixels in the drizzled image. For objects with $\Delta V_{0.5-3.0} > 2.5$, the range of FWHM found for objects in both the drizzled and undrizzled images is much larger, extending from small values typical of point sources all the way to FWHM ~ 15 pixels or so. Thus, it appears that $\Delta V_{0.5-3.0} \sim 2.5$ signals the transition from point sources to resolved sources.

Our detailed comparison between drizzled and undrizzled images of the WF2 chip in filters F439W and F555W shows that in the end the point sources identified are nearly identical. The largest difference found is in S/N , and results in more spurious objects being identified in the disk of NGC6027d and near the dust lane in NGC6027a in the undrizzled image than in the drizzled image. Although the pixel scale is different by a factor of two between the drizzled and undrizzled images, the results for the structure parameter are nearly identical for point source candidates in both images: Those objects with $0.5 < \Delta V_{0.5-3.0} < 2.5$ have FWHM values expected for point sources in both the drizzled and undrizzled images. Those objects with $\Delta V_{0.5-3.0} > 2.5$ have FWHM values typical of resolved objects. Thus, we conclude that for the dataset presented here, our point source detection algorithm is not significantly improved by the application of the drizzling technique.

We note that a recent study of the star cluster candidates in NGC 3610 by Whitmore et al. (2002) supports this conclusion. In a previous study of NGC 3610, Whitmore et al. (1997) used undithered images to identify point sources using an algorithm almost identical to the one used here. In the more recent study, Whitmore et al. (2002) drizzled together deeper exposures of NGC 3610. Even though the S/N and pixel scale were improved in the more recent images, the results of the new search were similar to the results of the original study. They found that 22 of 23 cluster candidates identified from the earlier images were recovered in the new images. Also, 11 new, previously unidentified clusters were discovered in the higher resolution images. However, the majority of these are within the disk of NGC 3610, and the authors attribute their detection to their ability to identify clusters in regions of higher background, which is likely because of the combination of improved S/N and pixel scale, not just because of the improved pixel scale.

2.3. Aperture Photometry of Point Sources

We performed circular aperture photometry of all point sources detected using the method described previously. For consistency with Gallagher et al. (2001), the photometry of each source was calculated using similar techniques. The technique used and the few differences between this study and Gallagher et al. (2001) are described here.

Each object was measured with the IRAF APPHOT package using a circular aperture of 2 pixel radius. The sky level for each object was determined by taking the median value in an

annulus of 7 pixel inner radius and 10 pixel outer radius centered on the object. A correction for charge transfer efficiency (CTE) was calculated for each object using the formulation given in Dolphin (2000). Photometry was measured at both dither positions for all point sources, the CTE correction was applied, and then the results for the two positions were averaged.

In order to transform the instrumental magnitudes to the standard VEGAMAG system, the zero points from Dolphin (2000)⁴ were adopted. These zero points were calculated using the standard $0''.5$ aperture, and therefore, aperture corrections need to be applied to our data to account for the different aperture size used.

Aperture corrections were calculated by photometering bright, isolated point sources in our 2 pixel aperture and in the 5.15 pixel, $0''.5$ aperture. The difference in magnitudes in these two measurements was calculated for each point source, and the mean adopted as the aperture correction. There were not enough point sources to solve for the aperture correction for each WF chip independently, so we adopt the same aperture correction for each chip. Table 2 lists the adopted values for the aperture correction in each filter, the number of objects used to derive the correction, and the standard deviation of the measurements.

The value for the Galactic extinction towards Seyfert’s Sextet was derived from the Schlegel et al. (1998) dust maps. The value returned was $E(B-V) = 0.055$, which is adopted as the foreground reddening towards all objects in the WFPC2 images of the Sextet. In order to determine the reddening corrections for the specific *HST* filters employed in this study, a synthesized instantaneous-burst star cluster model spectrum (the “BC95” models; Bruzual & Charlot 1993; Charlot, Worthey, & Bressan 1996) with an age of 10 Gyr (see §2.4) was reddened using a Cardelli et al. (1989) extinction law. Using the STSDAS SYNPHOT package, this reddened spectrum was convolved with the *HST* filter functions and the following corrections were calculated: $A_{F336W} = 0.270$, $A_{F439W} = 0.228$, $A_{F555W} = 0.171$, and $A_{F814W} = 0.101$. All of the point source photometry presented here has been corrected using these estimates for the Galactic reddening corrections.

2.4. Results of the Point Source Photometry

Figure 4 presents the calibrated photometry and associated measurement error for the 188 point sources identified in the three Wide Field chips. Among the 188 point sources detected, 106 were simultaneously detected in both V and I , 26 in B , V , and I , and only 5 were detected in all four filters. Figures 5 and 6 are the $V - I$ vs. V color–magnitude diagram (CMD) for the 106 sources detected in both filters and the $B - V$ vs. $V - I$ two–color diagram (2CD) for the 26 sources detected in all three filters.

⁴The functional form and coefficients for the CTE correction as well as the photometric zero points were taken from the website update to the published values, which is found at the following URL: www.noao.edu/staff/dolphin/wfpc2_calib/.

Although a correction for Galactic reddening was applied to the point source photometry, differential reddening due to the dust content of the compact group itself is also likely to affect the photometry of the point sources. For reference, a reddening vector equivalent to one magnitude of extinction in the F555W filter is plotted in Figures 5 and 6. Differential reddening is likely to be affecting many of the sources to some degree. However, because at least some of the point sources are found far from the outer isophotes of the giant galaxies, it is unlikely that there is a large, systematic shift in the colors and magnitudes of all of the sources.

If we assume that the differential reddening in the group is not severe, then one conclusion that can immediately be drawn from the CMD and the 2CD is that there are very few bright, blue point sources detected. Our choice of exposure times for the two blue filters was guided by observations of blue point sources in other studies of mergers (e.g., the Antennae, Whitmore et al. 1999) and compact groups (e.g., HCG92, Gallagher et al. 2001). Given our exposure times, the resulting limiting magnitude in B is brighter than our V limit (the magnitudes where the mean photometric error for point sources reaches 0.1 mag are 24.6, 25.0, and 24.3 for B , V , and I , respectively), however, the limits are such that we should have detected any objects with $B - V \lesssim 1.0$ and $V \lesssim 23.5$ in both filters. This observational selection effect does render us insensitive in B to faint point sources with $B - V \gtrsim 1.0$, however, the candidate young star clusters identified in other systems are all blueward of this limit.

In Seyfert’s Sextet, we find only a handful of objects are detected blueward of $V - I = 0.7$. The majority of the point sources detected have $0.7 < V - I < 1.3$ (which are likely to have $B - V \sim 0.7 - 1.0$), but most went undetected in B . This lack of bright, blue point sources in the Sextet is somewhat unexpected since these objects are found in abundance in similar systems. For example, in Gallagher et al. (2001), the peak in the color histograms for the identified point sources in Stephan’s Quintet (HCG92) are found at $B - V \sim 0.1$ and $V - I \sim 0.4$. Also, Johnson & Conti (2000) find a number of bright point sources in *HST* images of HCG31 that have $-1 < V - I < 0.4$ (the extremely blue objects in this sample are likely to have a large contribution to their flux from nebular line emission).

The 2CD for Seyfert’s Sextet point sources (Figure 6) also includes the evolutionary tracks derived from the BC95 (Bruzual & Charlot 1993; Charlot, Worthey, & Bressan 1996) solar metallicity instantaneous-burst stellar population models. In the CMD, the colors and magnitudes of these same BC95 models are included, where the magnitudes have been normalized for a cluster with masses of $10^5 M_\odot$ and $10^6 M_\odot$. There is a significant amount of scatter in the data for the star cluster candidates, however, the majority of the objects detected have colors in the 2CD similar to the expectations for clusters of 1 Gyr or older. In the CMD, the track for the $10^6 M_\odot$ clusters fits the data better than that of the lower mass model, and also indicates an age for the clusters in excess of 1 Gyr. Unlike the two previous studies of star cluster formation in compact groups (Johnson & Conti 2000; Gallagher et al. 2001), there does not appear to be any significant population of candidate young star clusters with ages less than 1 Gyr.

In Figure 7, we present histograms of the $V - I$ colors for the 106 point sources detected in both V and I (top panel) and the V magnitudes for the 84 likely cluster candidates in the restricted color range $0.5 < V - I < 1.5$ (bottom panel). The color and magnitude distributions presented in this Figure are consistent with our interpretation of an older population of globular clusters. The mean color of the objects in the Sextet with $0.5 < V - I < 1.5$ is 0.99, which is similar to the mean colors of the globular cluster populations in *HST* observations of ellipticals and S0s found by Kundu & Whitmore (2001a,b). The histogram of the V magnitudes of the likely cluster candidates identified in the Sextet is consistent with the luminosity function of the globular cluster populations seen in the deeper photometry of Kundu & Whitmore (2001b); some of the single elliptical galaxies in that study contain more clusters brighter than $V = -9$ than are found in the entire compact group studied here. However, since the observations presented in this paper were not designed to study the fainter old population of globular clusters in this compact group, it is likely that our census of the old clusters in the group is incomplete. Given the likely incompleteness, though, the data on the Sextet cluster candidates presented in Figure 7 are consistent with the standard (old) globular cluster luminosity function (Harris 2001), not just the *HST* data of Kundu & Whitmore (2001b).

Blue globular clusters are expected to be as bright or brighter than the older, red globular clusters (unless they are of much lower mass); for example, many of the blue clusters identified in NGC3256 (Zepf et al. 1999) have $M_I < -10$, which is above our detection threshold. Thus, Figures 5 and 7 should represent accurately the population of clusters in the Sextet; the population is truly dominated by red clusters. However, among the sources that were detected in B , V , and I , there are a few blue point sources observed, those on WF2 that have $V - I < 0.5$. Four of the five blue point sources are located within the disk of NGC6027d, and the fifth is just south of the disk (it is the southernmost point source visible in Figure 3). This region appears to be the only site that includes young, star-forming regions.

2.5. Extended Source Detection and Photometry

Hunsberger et al. (1998) have identified samples of dwarf galaxy candidates in a number of HCGs using the FOCAS software package (Jarvis & Tyson 1981) to perform star/galaxy separation on ground-based R band images. Seyfert’s Sextet was not included in this study, however, we present here (Figure 8) a previously unpublished, deep R band image of Seyfert’s Sextet observed after the conclusion of the HCG survey of Hunsberger et al. (1998). Although the majority of the HCGs in the Hunsberger et al. (1998) sample were observed with the Palomar 1.5m, this image was taken with the Kitt Peak 0.9m telescope in 1996 May. The data reduction and analysis techniques used to process this image were identical to those used in Hunsberger et al. (1998).

In Figure 8, a large circle indicates the boundary of the group; the radius of this circle is twice the size of the radius of the smallest circle that encloses the 23 mag arcsec⁻² isophotes of the giant galaxy members, $2 \times R_g$ (see Hunsberger et al. 1998), and within that boundary every non-stellar

object is indicated by an ellipse. Apart from the objects that make up the Sextet (five galaxies and the bright tidal tail), 33 objects were detected and classified as non-stellar. The majority of these objects are found in the northwest quadrant of the image, and several appear to be superposed on the fainter tidal tail, which extends to the northwest of NGC6027c.

Comparison to the *HST* image (Figure 2) reveals that the majority of the galaxies identified in the ground-based image of the Sextet are background galaxies. Viewed at higher angular resolution, many of the non-stellar objects appear to be background disk galaxies, and the two bright, red galaxies west of NGC6027c appear to be background giant ellipticals. However, several of the candidate dwarf galaxies do appear to be just that, dwarf galaxies associated with the Sextet. Furthermore, several faint, diffuse objects not visible in the ground-based image are also apparent in the *HST* image. In this section we will describe the identification and photometry of the extended sources observed in the *HST* image.

Detection of candidate dwarf galaxies associated with Seyfert’s Sextet is reasonably straightforward; assuming a distance modulus of 33.8, a typical dwarf galaxy will have $M_V = -14$, or a total magnitude of ~ 20 in the F555W filter. Furthermore, a dwarf galaxy with a core radius of ~ 300 pc will have an angular radius $> 1''$, and will therefore cover roughly 300 or so pixels. Thus, we expect most dwarf galaxies (including those fainter than $M_V = -14$) to be detected with high signal-to-noise in our F555W and F814W images. There are some limits, though; the photometric error is ~ 0.1 for point sources with $M_V < -9$, and the sensitivity of the WF chips to low surface brightness sources is limited. Thus, we do not expect to detect the faintest, diffuse dwarf galaxies, similar to the Local Group dwarf spheroidal galaxies (which are as faint as $M_V \sim -8$).

Selection of extended sources to photometer was accomplished using the FOCAS software package, however, we set the parameters in order to select relatively bright, extended sources. The catalogue was constructed to include all objects with a minimum area of 50 pixels (0.5 square arcseconds) with fluxes 2.5σ above the background. This catalogue did contain some obvious contaminants, including saturated stars and several resolved H II regions in NGC6027d and NGC6027e. These were removed by hand. Ultimately, we were left with 38 objects. Most of the objects identified in the ground-based image that are within the boundaries of the WFPC2 image were included, as well as a number of fainter objects not visible in Figure 8. The only objects identified in the ground-based image that were not recovered by the automated detection algorithm were those found very near the boundaries of the WF chips, where the images had been trimmed. We also note that in a few cases, objects identified from the ground as a single extended source were resolved into two extended sources in the *HST* images.

It is apparent by visual inspection that a number of the extended sources seen in Figure 2 are disk galaxies. We remove from further consideration as potential dwarf members of Seyfert’s Sextet those galaxies with clear spiral structure and those that appear to be edge-on spiral galaxies. We assume that these objects are background galaxies. For the final catalogue of candidate dwarf galaxies, we have photometered 29 objects; six from the WF2 chip, 17 from WF3, and six from

WF4. In addition, we have photometered six of the background spiral galaxies (the other three were found on the edges of two WF chips, in the region trimmed from the images during data reduction) for comparison to the sample of dwarf galaxy candidates. Figure 9 is a finding chart for the 29 dwarf galaxy candidates and six background spiral galaxies that were photometered; a contour plot of a smoothed version of Figure 2 (smoothed to reduce some of the noise in the fainter isophotes) is shown with square boxes marking each object in this sample.

For each extended object in the catalogue, the STSDAS task ELLIPSE was used to fit elliptical isophotes to the galaxy in the *HST* *I* image out to a semi-major axis where the signal to noise became too low for the fitting routine to work successfully. The ellipse parameters derived for each object from the *I* image were then used to calculate the object’s flux in the other filters. A value of the average background flux per pixel was calculated for each image. For each object, the total flux within the elliptical apertures was corrected by subtracting off the total background contribution within the aperture, assuming that this average background flux per pixel is flat across the image. After background subtraction, the total flux for each object was converted into a total magnitude using the adopted Dolphin (2000) zero points (which were corrected to infinite aperture using the standard 0.1 magnitude offset; Holtzman et al. 1995). Few objects were detected in either *B* or *U*, and those that were detected have low *S/N*. Figure 10 is a $V - I$ vs. V color magnitude diagram for the 29 extended sources in the final catalogue. All of the photometry has been corrected for Galactic reddening. For reference, the point sources from Figure 5 are plotted as well.

2.6. Results of the Extended Source Photometry

As noted previously, when viewed at higher angular resolution, many of the extended objects in the field of Seyfert’s Sextet seen in Figure 8 appear to be background galaxies rather than dwarf galaxies associated with this HCG. The photometric results for the extended sources (Figure 10) lend some credence to this supposition. The extended objects are not distributed randomly around the group, instead they appear concentrated to the northwest of the Sextet. While we lack information on the southeast quadrant for comparison (even if the PC data was analyzed, it covers significantly less area than the WF chips), the density of extended objects on WF3 is noticeably higher than on WF2 or WF4. As expected for a background cluster or group, the majority of the galaxies observed lie in a narrow region of parameter space, with $V - I > 1.5$ and $21 < V < 23$. The six extended sources that are obvious disk galaxies are also found in this same region of the color-magnitude diagram. In addition to the faint, red galaxies, there are three bright, red objects on WF3 ($V - I > 1.5$ and $V < 20.6$) that appear to be the massive elliptical galaxy members of a poor cluster or group.

Based on color alone it is difficult to say with certainty that the three bright ellipticals are giants and not dwarfs because the $V - I$ colors of dwarf galaxies and giant ellipticals can be similar. For dwarf galaxies, $V - I$ colors of $\sim 1 - 1.3$ are typical. For example, the Local Group dwarf ellipticals (dEs) NGC 147, NGC 185, and NGC 205 have $V - I = 1.12, 1.25, 1.23$ respectively

(Mateo 1998). In a recent study of low surface brightness dwarf galaxies in the Dorado Group, Carrasco et al. (2001) found 65 such objects with $V - I$ colors from -0.3 to 2.3 . This distribution had a strong peak at $V - I = 0.98$, again suggesting that this is a typical color for a dE galaxy. For giant elliptical galaxies (gEs), the typical $V - I$ color on average may be redder by a few tenths of a magnitude than that of a typical dE. For example, Carollo et al. (1997) observed a sample of 15 nearby ellipticals with *HST* and found a range of colors of $1.24 < V - I < 1.42$. Although the typical colors of gEs and dEs may only differ by a small amount, there is overlap in the overall distribution of colors between these two populations of galaxies. Thus, additional information besides the broadband colors is required to distinguish between a dE and a gE.

The majority of the galaxies identified in Figure 9 have colors redder than either the typical dE or gE. The amount of Galactic reddening towards Seyfert’s Sextet is low, and has already been removed from the colors plotted in Figure 10. Internal, differential reddening due to dust in the Sextet system is likely to affect the colors of the galaxies to some extent, but A_V of $2-3$ magnitudes is required to redden dwarf galaxies with $V - I \sim 1.0$ to $V - I > 1.5 - 2.0$. Since the majority of the galaxies photometered are located outside of the bright isophotes of the Sextet galaxies, it is unlikely that they are being reddened to such a significant extent.

The assumption that the majority of the faint, red galaxies observed (including the six background spiral galaxies, which have red $V - I$ colors) are members of a background cluster provides a convenient explanation for the red colors of these galaxies without invoking significant internal reddening. Assuming that the three bright ellipticals are giant ellipticals, then the redshift of this group is likely to be $z > 0.3$ so that $M_V < -20.5$ for these objects. At $z = 0.32$, the k correction to the $V - I$ color is ~ 0.67 magnitudes for an elliptical galaxy and ~ 0.40 magnitudes for an SA galaxy (Poggianti 1997). Thus, we expect an elliptical at $z \sim 0.3$ to have $V - I \sim 1.9 - 2.1$, which is similar to the colors of the ellipticals found in our sample.

Perhaps the strongest evidence that these three bright, red objects are not dwarf galaxies but are instead giant galaxies comes from their surface brightness profiles. Figure 11 presents I band surface brightness profiles for the two brightest ellipticals, which are labeled objects 3.9 and 3.15 on the finding chart (Figure 9). The third bright elliptical (galaxy 3.16) is fainter than galaxies 3.9 and 3.15 by more than a magnitude, and its profile was not fit because the lower signal to noise surface photometry resulted in a poorly constrained fit. The two brightest elliptical galaxies are fit well by Sérsic profiles of the form:

$$\mu(r) = \mu_0 + 1.0856(r/r_0)^n \quad (1)$$

where μ is the F814W surface brightness in mag arcsec^{-2} and n is fixed at $1/4$ (i.e., the de Vaucouleurs law). In Figure 11, these $r^{1/4}$ law fits are overplotted on the surface brightness data, showing the goodness of fit. For galaxy 3.9, the fitted central surface brightness, μ_0 , is 15.6 ± 1.0 mag arcsec^{-2} and for galaxy 3.15, $\mu_0 = 15.1 \pm 1.2$ mag arcsec^{-2} . Recent studies of dwarf galaxies in Virgo (Durrell 1997; Bingeli & Jerjen 1998) have shown that $r^{1/4}$ law fits are inappropriate

for dE galaxies; instead, the “shape parameter”, n , is allowed to vary, and dEs show a correlation between total magnitude and n . The range in n in dEs is found to be $0.4 < n < 2.0$ in both studies. Thus, the goodness of fit of an $r^{1/4}$ law to galaxies 3.9 and 3.15 is evidence that they are unlikely to be dEs. Furthermore, the central surface brightnesses of Virgo dEs ranges from 17.8 to 24.9 in R (Durrell 1997) and from 18.1 to 25.3 in B (Binggeli & Jerjen 1998). We conclude that both the shapes and central surface brightnesses of galaxies 3.9 and 3.15 are consistent with their being background gE galaxies rather than dEs associated with Seyfert’s Sextet.

Among the sample of extended objects, there are eight galaxies with $V - I$ colors less than 1.2, similar to the typical values for known dEs, and thus these objects are considered candidate dwarf galaxies. Table 3 includes the names and photometric results for these eight objects. Among these eight galaxies, six are simply faint ($V \lesssim 22$), blue ($V - I < 1.2$) galaxies. One of these six (galaxy 2.6) lies near the edge of the disk of NGC6027d, while two others (galaxies 4.1 and 4.3) lie near the bright tidal tail associated with NGC6027b. Galaxy 3.8 is a faint, blue galaxy that is found among the galaxies that form the suspected background cluster or group on WF3. However, it is found just outside of the isophotes of the tidal tail that extends from NGC 6027c. Galaxy 3.10 is also found among the suspected background cluster, but is further from the tidal feature. Galaxy 4.6 may be a background spiral, but the spiral structure is not clear enough to definitively classify this object as a disk galaxy.

Besides the six faint, blue dwarf galaxy candidates there are two objects with more irregular morphologies. Galaxy 4.2 is a bright, blue galaxy that shows obvious signs of star formation in the form of several compact, bright point sources superposed on a faint, S-shaped continuum. This object’s morphology is reminiscent of the class of blue compact dwarfs (see, e.g., Papaderos et al. 1996). Galaxy 3.14 is an irregularly shaped, extended object seen quite close to the disk of NGC6027c.

In addition to the color selected candidates, we include one other galaxy in Table 3 as a possible dwarf galaxy candidate. Galaxy 3.3 is one of the “faint, red” galaxies found on chip WF3. However, this galaxy is found within the boundaries of the faint tidal tail associated with NGC6027c, and it has a very peculiar morphology. This object appears to have a “cometary” morphology, with an elliptical galaxy at the “head” and a narrow “tail” of emission extending to the south of the head. This galaxy appears to be a single, distorted galaxy, however, we note that a more nearby pair of galaxies exhibit a similar appearance. The system Arp 296 (see Hibbard & Yun 1999, for a B band image) is a face-on disk galaxy and a thin, edge-on disk galaxy that may be similar to galaxy 3.3. If galaxy 3.3 is a system like Arp 296, then it is most likely a background object rather than a dwarf galaxy associated with the Sextet.

These nine candidate dwarf galaxies stand out among the sample of extended objects because of their colors, and also, in the three specific cases described previously, because of their morphologies. It is interesting that many of these faint galaxies lie in or near the tidal features associated with the Sextet, however, this may be coincidental since the Sextet galaxies fill much of the area of the three

WF chips. In the end, we refer to these galaxies as candidate dwarfs, since redshift information is necessary to discriminate between the possibilities that they are dwarf galaxies in the Sextet or are background galaxies.

We hypothesized that the majority of the faint, red galaxies observed are members of a group or cluster seen in projection against Seyfert’s Sextet. The observations indicate that the bright, red elliptical galaxies are background giant ellipticals rather than dwarf ellipticals. However, there is little direct evidence that all of the faint, red galaxies are also background objects; certainly the colors (assuming a relatively significant k correction) and morphologies of the objects *support* the hypothesis that these objects are background objects, but they do not prove the hypothesis. It is possible that some of the red galaxies may be dwarf galaxy members of Seyfert’s Sextet, but it does seem more likely that the majority are background galaxies.

3. Spectroscopy of a Tidal Dwarf Candidate

During 2002 March, spectroscopic follow-up observations of a number of galaxies identified in the *HST* images of Seyfert’s Sextet were undertaken with the Hobby-Eberly Telescope (Ramsey, Sebring, & Sneden 1994). The observations were made with the Marcario Low-Resolution Spectrograph (Hill et al. 1998; Schneider et al. 2000) in multi-object mode. Three 800 second exposures were obtained and subsequently averaged together. Unfortunately, observing conditions were such that only one spectrum (galaxy 4.2) was extracted with reasonable signal-to-noise.

The observations were obtained with a 600 line mm^{-1} grism used in conjunction with 1'3 slitlets to provide resolution of $R \sim 1000$. Wavelength calibration for the spectrum was determined from both HgCdZn and Neon comparison lamp exposures; the resulting wavelength calibrated spectrum covers $\sim 4000 - 6900 \text{ \AA}$. Figure 12 shows the wavelength calibrated spectrum of galaxy 4.2 over the range $4000 - 6000 \text{ \AA}$.

Although a weak continuum is detected, the spectrum does contain four emission lines; $\text{H}\beta$ and the $[\text{O III}] \lambda\lambda 4959, 5007$ doublet are observed at high signal-to-noise, while $\text{H}\gamma$ is detected with marginal significance. These lines and the observed wavelengths for each (derived from Gaussian fits to the line profiles) are listed in Table 4.

The mean redshift for the accordant galaxies in Seyfert’s Sextet is $v = cz = 4347 \text{ km s}^{-1}$ (Hickson et al. 1992). The emission lines provide a redshift for this dwarf galaxy candidate of $v = cz \sim 20,000 \text{ km s}^{-1}$, placing it in the background behind Seyfert’s Sextet. However, it is interesting to note that this galaxy has a redshift almost identical to that of NGC6027e, the discordant spiral in the Sextet, which has a redshift of $19,809 \text{ km s}^{-1}$ (Hickson et al. 1992). Adopting $z = 0.067$ for NGC 6027e and galaxy 4.2, the distance to these two galaxies is approximately $260 h_{75}^{-1} \text{ Mpc}$. The absolute V and I magnitudes of galaxy 4.2 are approximately -16.7 and -17.4 respectively. The projected separation between these two galaxies is roughly $80''$, which at the adopted distance is $< 100 \text{ kpc}$. Thus, we suggest that galaxy 4.2 may be a dwarf galaxy satellite

of NGC6027e.

4. Discussion and Conclusions

The case study of Seyfert’s Sextet presented here is part of a continuing effort to determine whether dwarf galaxies form during tidal interactions among giant galaxies. The Sextet appears to be the most logical choice to search for tidal dwarf formation; it is the most compact of the Hickson compact groups, contains two prominent tidal tails, has a low velocity dispersion, and previous ground-based imaging revealed a number of faint, extended objects within the boundaries of the group. However, the results of the *HST* imaging of Seyfert’s Sextet show that, contrary to expectations, there is very little evidence for dwarf galaxy formation or any other strong star formation in this group.

A large number of both point sources and extended sources were catalogued and photometered from the three Wide Field images. We find that very few objects are detected in either of the two blue filters, F336W and F439W, and those that are detected in the two red filters, F555W and F814W, have red colors consistent with those of old stellar populations. The majority of the point sources detected appear to be old (> 1 Gyr) and the majority of the extended sources detected appear to be background galaxies.

These photometric results contrast sharply with *HST* imaging studies of other HCGs, such as HCG92 (Stephan’s Quintet) and HCG31. In HCG92, Gallagher et al. (2001) found a number of bright, blue star cluster candidates in the tidal debris regions of this group. The images of this compact group also show bright, blue extended sources in the “Northern Starburst Region” and in the tidal tails of NGC7319 and NGC7318a/b. HCG31 contains a significant number of bright, blue point sources (Johnson & Conti 2000) similar to those seen in HCG92. Star-forming regions are also observed in HCG31 that are “too small to be called galaxies themselves, but are not clearly associated with either galaxy AC or galaxy E” (Johnson & Conti 2000). Thus, both HCG92 and HCG31 contain what appear to be young star clusters and tidal dwarf galaxy candidates, while Seyfert’s Sextet does not appear to contain a significant population of either type of object.

The star cluster candidates identified in this study have photometric properties consistent with those for models of massive ($\sim 10^6 M_\odot$) clusters with ages $10^{8.5} - 10^{9.5}$ years. The ages of these objects suggest that they are not entirely a primordial population, but may be the product of an interaction within the compact group at some time within the past few Gyr. Williams, McMahon, & van Gorkom (1991) argue that the optical tail associated with NGC 6027b and the H I gas that they associate with NGC 6027d may have resulted from an interaction between these two disk galaxies more than 5×10^8 years ago. The ages we derive for many of the cluster candidates are consistent with this hypothesis.

While there do not appear to be any young star clusters or tidal dwarf galaxies associated with Seyfert’s Sextet, we did identify several candidate dwarf galaxies in the group. This sample includes

a few faint, blue extended sources, and two galaxies with peculiar morphologies: an irregularly shaped galaxy located quite near the disk of NGC6027c and an unusual, “cometary” galaxy located within the tidal tail associated with NGC6027c. An additional candidate, galaxy 4.2, has already been ruled out as a member of the Sextet; the Hobby-Eberly Telescope spectrum of this object instead shows that it is associated with NGC6027e, the discordant redshift member of Seyfert’s Sextet. Whether or not the other candidate dwarf galaxies are associated with the Sextet, they appear morphologically very different from the clumpy, blue tidal dwarf galaxy candidates in HCG92 and HCG31.

The data suggest that there is some fundamental, physical difference between the Sextet and the two HCGs that are known to contain young star clusters and tidal dwarf galaxy candidates. One obvious difference between these groups are the types of galaxies contained in each: Seyfert’s Sextet is primarily made up of early-type (S0/E) galaxies, Stephan’s Quintet contains spirals, and HCG31 contains mostly irregular galaxies. Based on these morphologies, one initial expectation is that the neutral gas content in Seyfert’s Sextet is likely to be lower than that of either HCG31 or HCG92. Radio observations show that the Sextet contains only $2 \times 10^9 M_{\odot}$ of neutral Hydrogen (Verdes-Montenegro et al. 2001), about an order of magnitude less than that of HCG31 and HCG92 (Williams, McMahon, & van Gorkom 1991; Verdes-Montenegro et al. 2001). The most recent observations of the gas content of HCG92 (Williams, Yun, & Verdes-Montenegro 2002) revise the gas mass of this group downward, however it remains at least five times larger than the gas in Seyfert’s Sextet.

What appears to be the more significant difference among these three HCGs, however, isn’t the gas mass, but the *distribution* of the H I. Williams, McMahon, & van Gorkom (1991) present VLA neutral Hydrogen observations of Seyfert’s Sextet that indicate that the majority of the H I mass is retained by the disk of NGC6027d, although some gas is found in a tail extending to the east of this galaxy and also in the optical tidal tail associated with NGC6027b. In HCG31, the VLA neutral Hydrogen maps (Williams, McMahon, & van Gorkom 1991) show that the gas is found both in the galaxies themselves and in a large envelope of gas that is plausibly attributed to tidal interactions between the galaxies. The distribution of H I in HCG92 is found to lie entirely outside of the galaxies (Verdes-Montenegro et al. 2001; Williams, Yun, & Verdes-Montenegro 2002), however. The H I is concentrated in clouds and tidal tails that are not coincident with the disks of the member galaxies.

Verdes-Montenegro et al. (2001) proposed an evolutionary sequence based on their VLA observations of the H I content of HCGs. In their model, “phase 1” HCGs are those where the vast majority of the neutral gas remains bound to the member galaxies. “Phase 2” HCGs are more evolved in the sense that the galaxies retain some of the gas, while approximately half of the gas mass is found in tidal features. The final, most evolved phase is broken into two subclasses, “phase 3a” and “phase 3b”. Phase 3a groups are those where the gas is almost completely stripped from the galaxies and is found entirely within tidal features, while phase 3b groups are a few rare cases where the entire group seems to be contained in a single H I cloud. HCG31 is considered a pro-

tototype phase 2 group, and HCG92 is considered an extreme example of phase 3a. Both Williams, McMahon, & van Gorkom (1991) and Verdes-Montenegro et al. (2001) find Seyfert’s Sextet to be anomalous; its gas distribution suggests that the system has not experienced significant dynamical evolution, while optical observations suggest the opposite.

We propose one possible scenario for the history of Seyfert’s Sextet that takes into account the following significant factors: (1) The tidal tails are evidence for interactions among the accordant redshift members some time in the past, (2) the interactions that have occurred have not triggered star and/or star cluster formation similar to that seen in other merging galaxies and compact groups, (3) the relatively small amounts of neutral gas in Seyfert’s Sextet remains bound in the one late type galaxy and does not appear to be distributed among the group environment, and (4) the low velocity dispersion among the member galaxies and the small distances between the member galaxies suggests that future interactions among the galaxies are likely. This accumulated evidence suggests that a number of gas-poor (and one gas-rich) galaxies have interacted beginning perhaps as long as 1 Gyr or more in the past (dated by the colors of the red globular cluster candidates). The interactions in the group have created the optical tidal tails and perhaps created the elliptical member of the Sextet, NGC6027a, as well. The interactions in the past stripped stars from the progenitor galaxies, redistributing them within the group. The evidence for a red, low surface brightness halo encompassing all of the member galaxies, which is seen in our images as well as deeper ground-based images, is further evidence for a redistribution of the galaxies’ stars within the group. The only ongoing star formation and most of the neutral gas is found within the disk of NGC6027d, the only late type member of the group, suggesting that any interaction that involved this galaxy must have been minor, although the galaxy disk does appear somewhat irregular and perhaps warped.

We speculate that further interactions are probably inevitable, and a major interaction between NGC6027d and the other members of the group may trigger the stripping of its neutral gas and star cluster formation throughout the group in the future. Moreover, the low velocity dispersion suggests that none of the four large galaxies are likely to escape the group, and thus the group members may merge into a single galaxy, rather than remaining distinct. Thus, we believe that we are seeing Seyfert’s Sextet at the “beginning of the end”; we presume that the future interactions will be the end of this group, transforming it into a single galaxy.

We wish to acknowledge the help of M. Eracleous with data reduction of our HET spectra. We also wish to thank J. Hibbard for a number of useful discussions. SZ acknowledges support from the National Science Foundation through a Research Experiences for Undergraduates award. This work was supported by NASA STScI and by the NSF under grants NSF AST 00-71223 and STSI HST-GO-08717.04-A.

REFERENCES

- Barnes, J. E. & Hernquist, L. 1992, *Nature*, 360, 715
- Binggeli, B. & Jerjen, H. 1998, *A&A*, 333, 17
- Bruzual, G. A. & Charlot, S. 1993, *ApJ*, 405, 538
- Cardelli, J. A., Clayton, G. C. & Mathis, J. S. 1989, *ApJ*, 345, 245
- Carrasco, E. R., Mendes de Oliveira, C. L., Infante, L., & Bolte, M. 2001, *AJ*, 121, 148.
- Carollo, C. M., Franx, M., Illingworth, G. D., & Forbes, D. A. 1997, *ApJ*, 481, 710.
- Charlot, S., Worthey, G., & Bressan, A. 1996, *ApJ*, 457, 625
- Deeg, H. J., Munoz-Tunon, C., Tenorio-Tagle, G., Telles, E., Vilchez, J. M., Rodriguez-Espinosa, J. M., Duc, P. A., & Mirabel, I. F. 1998, *A&AS*, 129, 455
- Dolphin, A. E. 2000, *PASP*, 112, 1397
- Duc, P.-A., Brinks, E., Springel, V., Pichardo, B., Weilbacher, P., & Mirabel, I. F. 2000, *AJ*, 120, 1238
- Duc, P.-A. & Mirabel, I. F. 1998, *A&A*, 333, 813
- Durrell, P. R. 1997, *AJ*, 113, 531
- Elmegreen, B. G., Kaufman, M., & Thomasson, M. 1993, *ApJ*, 412, 90
- Fruchter, A. S. & Hook, R. N. 2002, *PASP*, 114, 144
- Gallagher, S. C., Charlton, J. C., Hunsberger, S. D., Zaritsky, D., & Whitmore, B. C. 2001, *AJ*, 122, 163
- Harris, W. E. 1996, *AJ*, 112, 1487
- Harris, W. E. 2001, in *Saas-Fee Advanced Course 28, Star Clusters*, ed. B. W. Carney et al. (New York: Springer), 223
- Hibbard, J. E., Guhathakurta, P., van Gorkom, J. H., & Schweizer, F. 1994, *AJ*, 107, 67
- Hibbard, J. E., van der Hulst, J. M., Barnes, J. E., & Rich, R. M. 2001, *AJ*, 122, 2969
- Hibbard, J. E. & Yun, M. S. 1999, *AJ*, 118, 162
- Hickson, P. 1982, *ApJ*, 255, 382
- Hickson, P. 1994, *Atlas of Compact Groups of Galaxies*, (Basel: Gordon and Breach Science Publishers)

- Hickson, P. 1997, *ARA&A*, 35, 357
- Hickson, P., Mendes de Oliveira, C., Huchra, J. P., & Palumbo, G. G. 1992, *ApJ*, 399, 353
- Hill, G. J., Nicklas, H. E., MacQueen, P. J., Tejada, C., Cobos Duenas, F. J., & Mitsch, W. 1998, *Proc. SPIE*, 3355, 375
- Holtzman, J. A. et al. 1992, *AJ*, 103, 691
- Holtzman, J. A., Burrows, C. J., Casertano, S., Hester, J. J., Trauger, J. T., Watson, A. M., & Worthey, G. 1995, *PASP*, 107, 1065
- Hunsberger, S. D., Charlton, J. C., & Zaritsky, D. 1996, *ApJ*, 462, 50
- Hunsberger, S. D., Charlton, J. C., & Zaritsky, D. 1998, *ApJ*, 505, 536
- Jarvis, J. F. & Tyson, J. A. 1981, *AJ*, 86, 476
- Johnson, K. E. & Conti, P. S. 2000, *AJ*, 119, 2146
- Kundu, A. & Whitmore, B. C. 2001a, *AJ*, 122, 1251.
- Kundu, A. & Whitmore, B. C. 2001b, *AJ*, 121, 2950.
- Mateo, M. 1998, *ARA&A*, 36, 435
- Mendes de Oliveira, C. L., Plana, H., Amram, P., Balkowski, C., & Bolte, M. 2001, *AJ*, 121, 2524
- Miller, B. W., Whitmore, B. C., Schweizer, F., & Fall, S. M. 1997, *AJ*, 114, 2381
- Mirabel, I. F., Dottori, H., & Lutz, D. 1992, *A&A*, 256, L19
- Mirabel, I. F., Lutz, D., & Maza, J. 1991, *A&A*, 243, 367
- O’Connell, R. W., Gallagher, J. S., Hunter, D. A., & Colley, W. N. 1995, *ApJ*, 446, L1
- Papaderos, P., Loose, H.-H., Thuan, T. X., & Fricke, K. J. 1996, *A&AS*, 120, 207.
- Poggianti, B. M. 1997, *A&AS*, 122, 399.
- Ramsey, L. W., Sebring, T. A., & Sneden, C. A. 1994, *Proc. SPIE*, 2199, 31
- Schlegel, D. J., Finkbeiner, D. P., & Davis, M. 1998, *ApJ*, 500, 525
- Schneider, D. P. et al. 2000, *PASP*, 112, 6
- Schweizer, F., Miller, B. W., Whitmore, B. C., & Fall, S. M. 1996, *AJ*, 112, 1839
- Seyfert, C. K. 1951, *PASP*, 63, 72

- Seyfert, C. K. 1948, *AJ*, 53, 203
- Stetson, P. B. 1987, *PASP*, 99, 191
- Verdes-Montenegro, L., Yun, M. S., Williams, B. A., Huchtmeier, W. K., Del Olmo, A., & Perea, J. 2001, *A&A*, 377, 812.
- Whitmore, B. C., Miller, B. W., Schweizer, F., & Fall, S. M. 1997, *AJ*, 114, 1797
- Whitmore, B. C., Schweizer, F. ;., Kundu, A., & Miller, B. W. 2002, *AJ*, 124, 147
- Whitmore, B. C., Schweizer, F., Leitherer, C., Borne, K., & Robert, C. 1993, *AJ*, 106, 1354
- Whitmore, B. C., Zhang, Q., Leitherer, C., Fall, S. M., Schweizer, F. ;., & Miller, B. W. 1999, *AJ*, 118, 1551
- Williams, B. A., McMahon, P. M., & van Gorkom, J. H. 1991, *AJ*, 101, 1957
- Williams, B. A., Yun, M. S., & Verdes-Montenegro, L. 2002, *AJ*, 123, 2417.
- Zepf, S. E., Ashman, K. M., English, J., Freeman, K. C., & Sharples, R. M. 1999, *AJ*, 118, 752

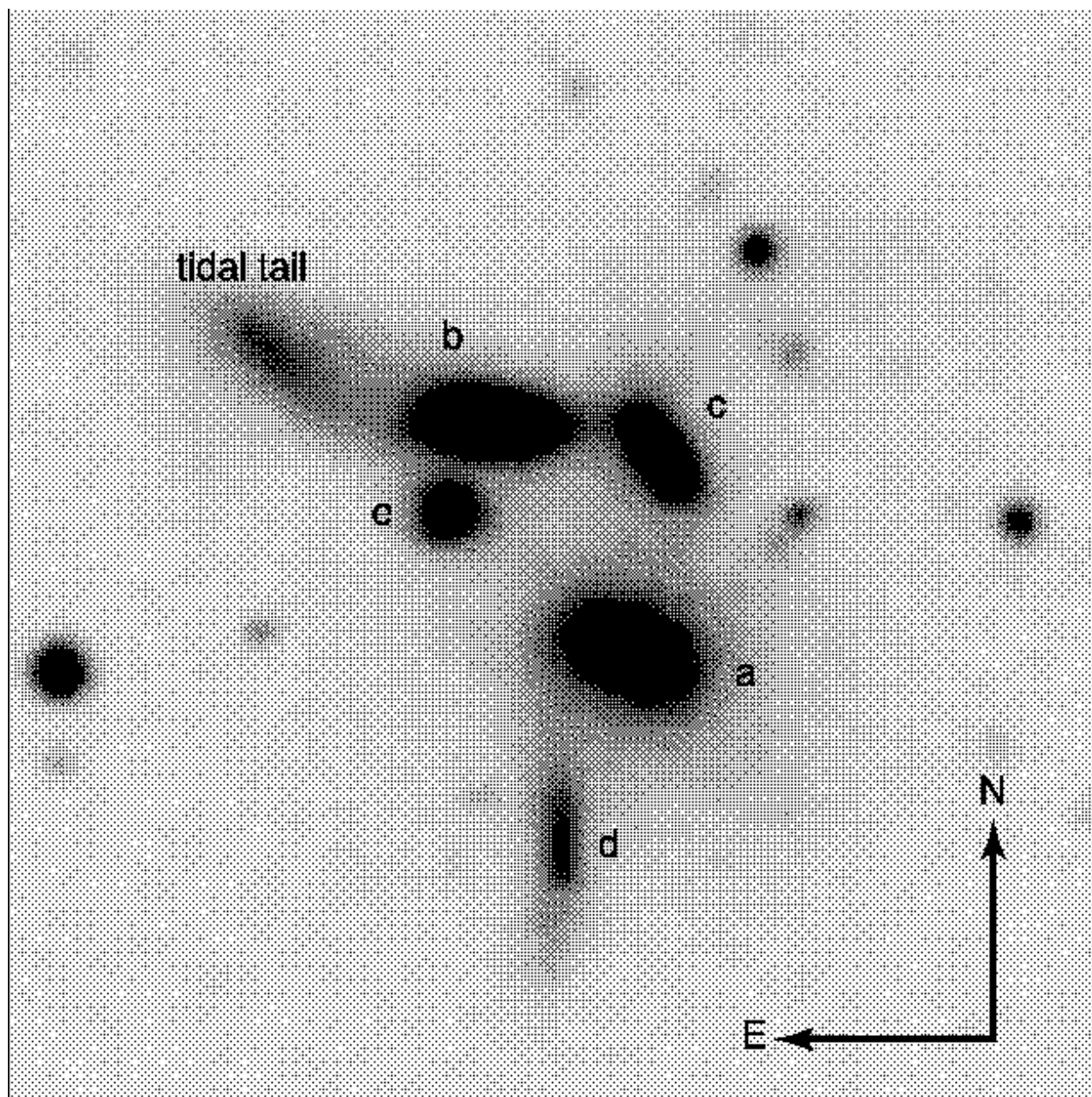


Fig. 1.— An image of Seyfert’s Sextet taken from the second generation Digitized Sky Survey (the red plate). This image is $5'$ on a side and north is up, east to the left. The individual galaxies, NGC6027a-e, are labeled using the notation of Hickson (1982). The bright tidal tail associated with NGC6027b is also labeled. There is another, fainter tidal tail associated with NGC6027c, but it is not seen in this image.



Fig. 2.— A natural color image of Seyfert’s Sextet created by combining the black and white data taken through the four WFPC2 filters, F336W, F439W, F555W, F814W (*UBVI*). Colors assigned to these data approximate the peak wavelengths of each filter: F336W data were colored reddish-violet, F439W blue, F555W yellowish-green, and F814W red. The inclusion of the ultraviolet filter causes the disk of NGC6027e, as well as the central regions of the edge-on spiral, NGC6027d, to be rendered more pink than they would be if strictly optical filters were used.

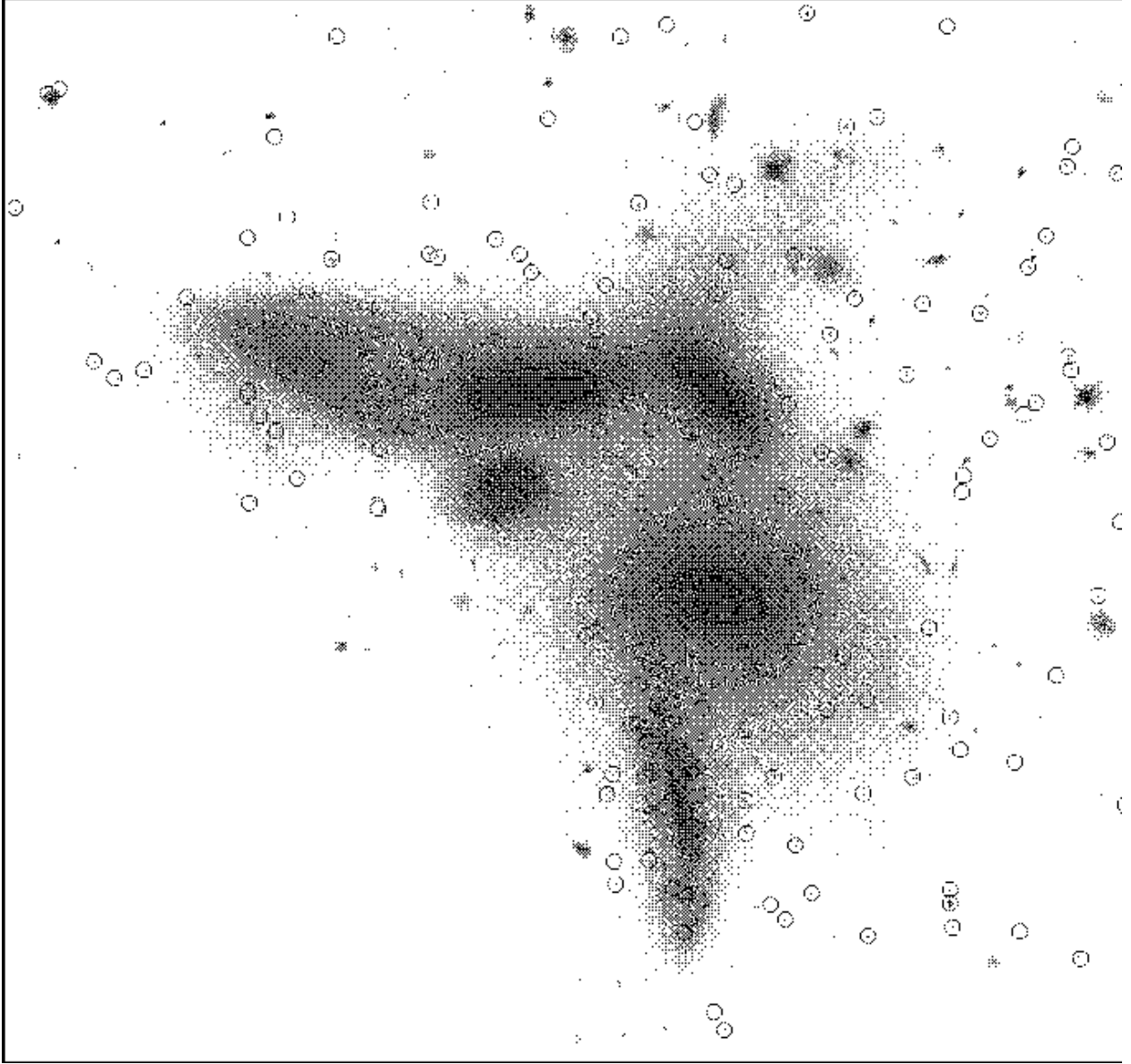


Fig. 3.— A finding chart for the 188 star cluster candidates identified on the three Wide Field chips. This image is a logarithmically scaled version of Figure 2, which has been binned by a factor of 2 in x and y for image compression purposes. A few sources are partially or completely outside of the boundaries of this slightly cropped image. North is up, and east to the left.

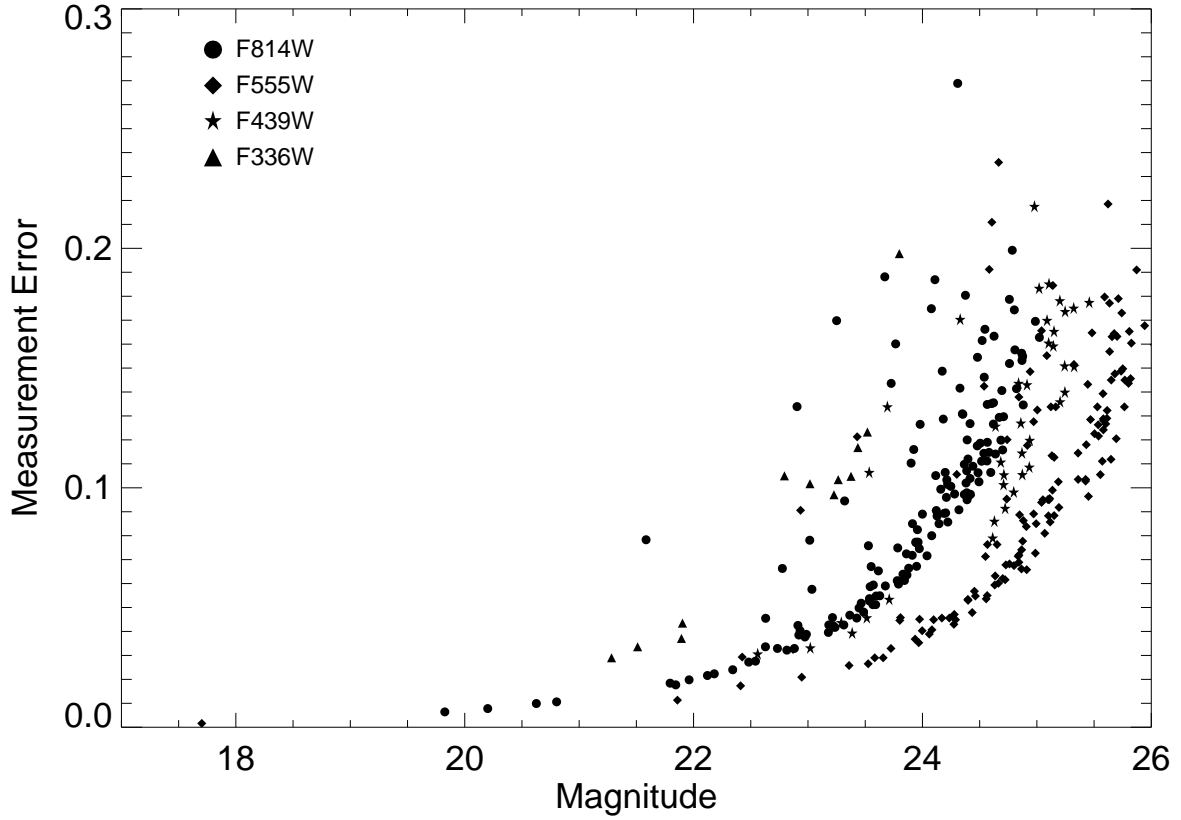


Fig. 4.— A plot of photometric error (in magnitudes) for the point sources identified in the three Wide Field Camera chips. This error only reflects measurement error, and does not include the contribution from the transformation to the standard system or the CTE correction. Different symbols are used for each filter: F814W data are the filled circles, F555W diamonds, F439W stars, and F336W triangles.

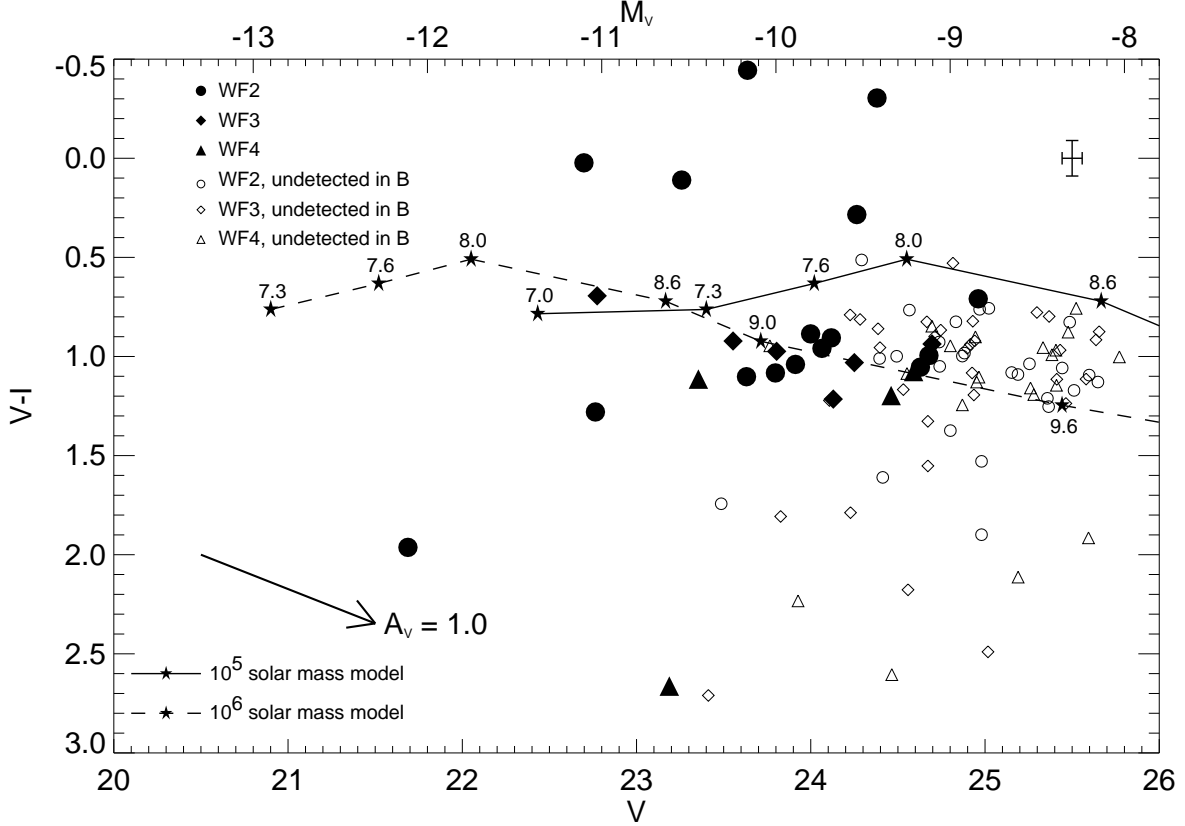


Fig. 5.— Color-magnitude diagram for all point sources detected in V (F555W) and I (F814W). All point sources detected in B , V , and I are plotted with filled symbols: circles for objects on Wide Field chip 2, diamonds for Wide Field chip 3, and triangles for Wide Field chip 4. Those objects detected in V and I but not detected in B are plotted as open symbols with the same symbol shapes reflecting chip location. A reddening vector is included for reference (lower left) as is the mean error in the photometry for the filled symbols (upper right). All of the photometry has been corrected for foreground Galactic reddening assuming $E(B - V) = 0.055$. The absolute magnitude scale is given assuming a distance to the Sextet of $57.5 h_{75}^{-1}$ Mpc. The two sets of solid stars plotted indicate the colors and magnitudes for an instantaneous-burst stellar population synthesis model (Charlot, Worthey, & Bressan 1996) of various ages; the points connected with the solid line and the dashed line are for models with total masses of $10^5 M_\odot$ and $10^6 M_\odot$, respectively. The model points are labeled with the logarithm of the age of the model, in years. The colors of the model stellar population are independent of the cluster mass, however changes in cluster mass will shift the model points by one magnitude for each factor of 2.5 change in the mass.

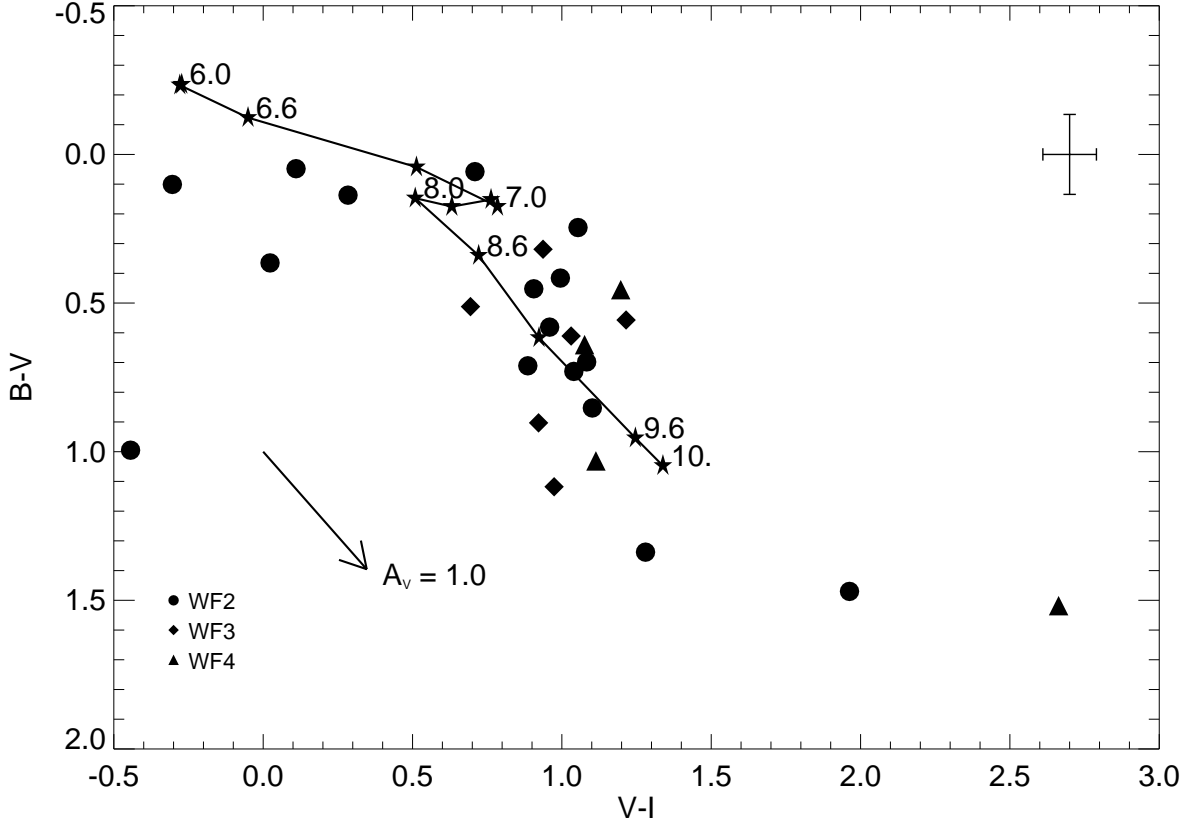


Fig. 6.— Color-color diagram for all point sources detected in B (F439W), V (F555W), and I (F814W). All of the photometry has been corrected for foreground Galactic reddening assuming $E(B - V) = 0.055$. Symbols are as in Figure 5. A reddening vector and error bars representing the mean error for the objects plotted are included for reference. The solid stars indicate the colors for an instantaneous-burst stellar population synthesis model (Charlot, Worthey, & Bressan 1996) of various ages. Several of the points are labeled with the logarithm of the age of the model, in years.

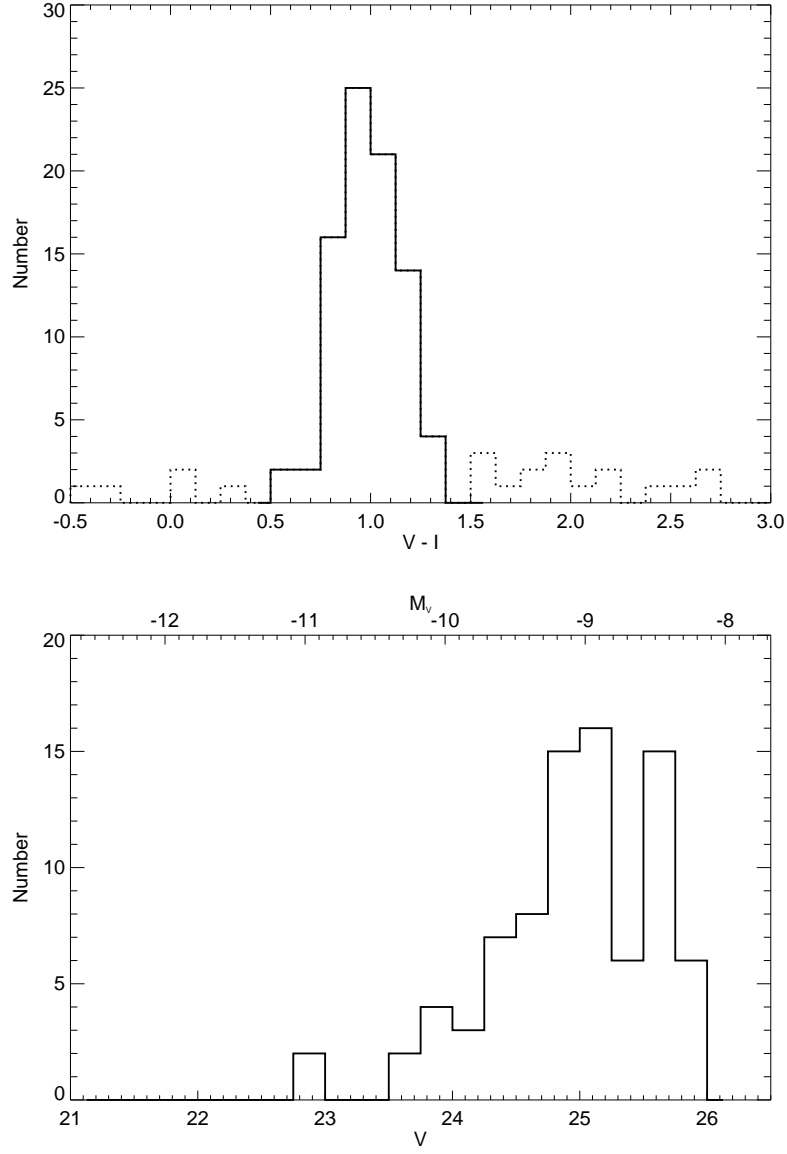


Fig. 7.— Histograms of the $V - I$ colors for 106 point sources detected on the WF chips (top panel) and V magnitudes for the 84 likely cluster candidates in the restricted color range $0.5 < V - I < 1.5$ (bottom panel). The bins of $V - I$ color represented by the dotted line in the top panel represent those objects that were excluded from the V magnitude histogram in the bottom panel.

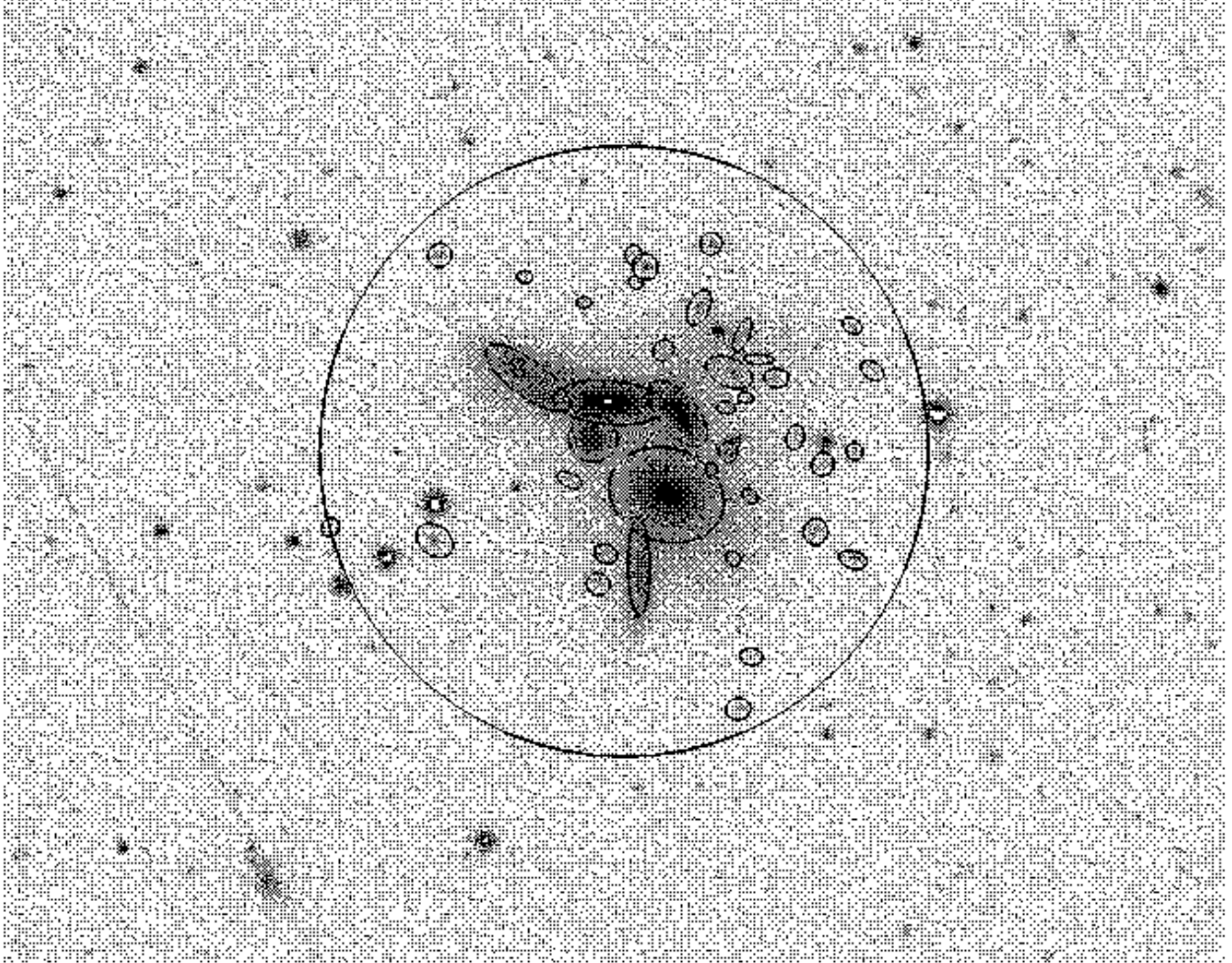


Fig. 8.— Kitt Peak 0.9m image of Seyfert’s Sextet. Ellipses represent extended objects detected with the FOCAS software. The large circle is constructed with a radius twice the size of the radius of the smallest circle that just encloses the $23 \text{ mag arcsec}^{-2}$ isophotes of the giant galaxy members of the Sextet.

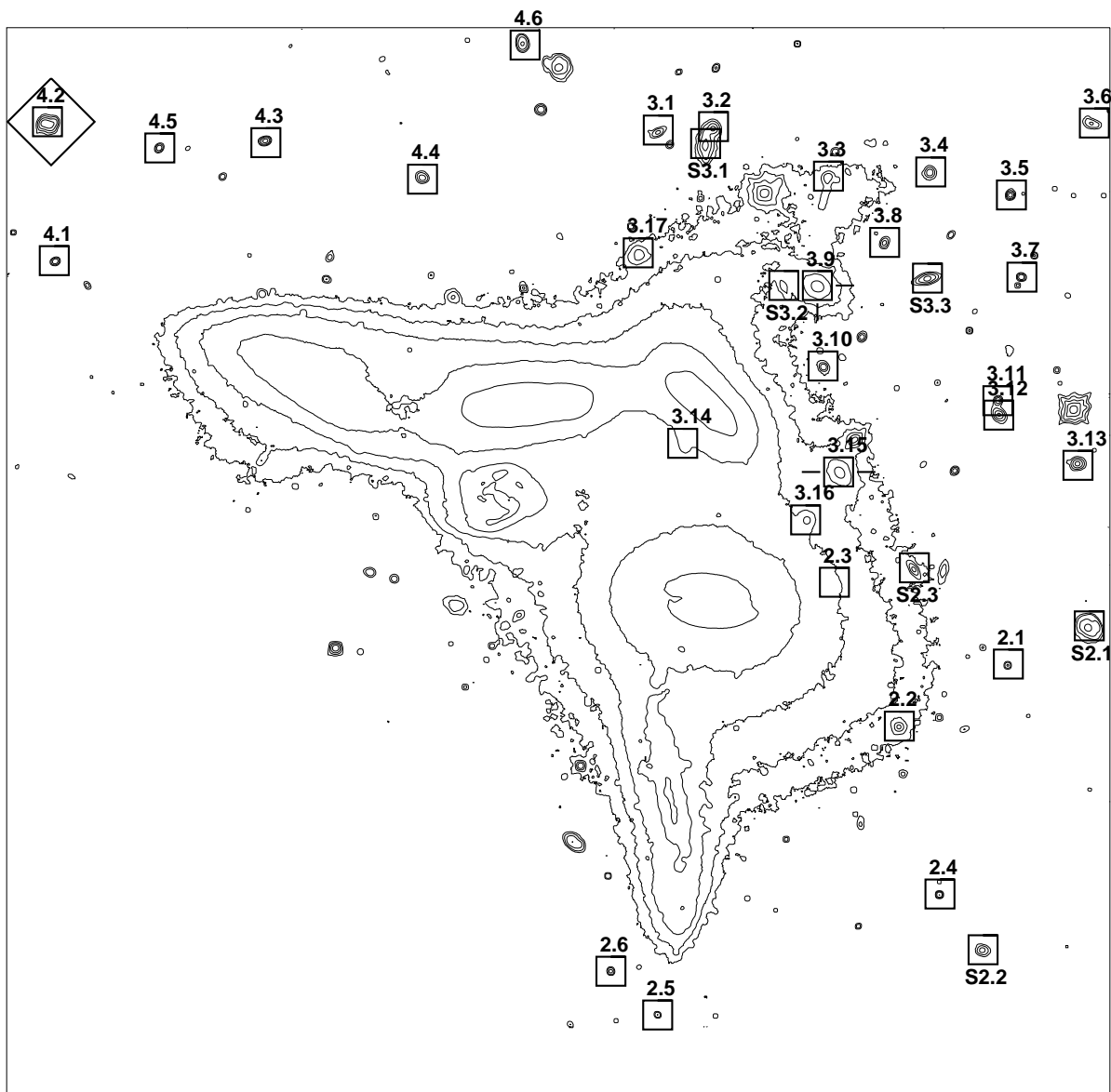


Fig. 9.— Finding chart for the 29 candidate dwarf galaxies and seven background spiral galaxies that were photometered. The image displayed in Figure 2 was smoothed with a 3 pixel boxcar averaging function to reduce some of the noise in the fainter isophotes and then contoured. Each galaxy that was photometered is marked with a large square and is labeled with an identifying number. For the dwarf galaxy candidates, the identifier is of the form X.X, where the first number is the WF chip and the second number is a sequence number. The background spirals are given identifiers of the form SX.X. A redshift has recently been obtained for Galaxy 4.2 (indicated by the large, open diamond) with the Hobby–Eberly Telescope; see §3. Surface brightness profiles for the two bright, red ellipticals (objects 3.9 and 3.15, indicated by two dashes) are presented in Figure 11.

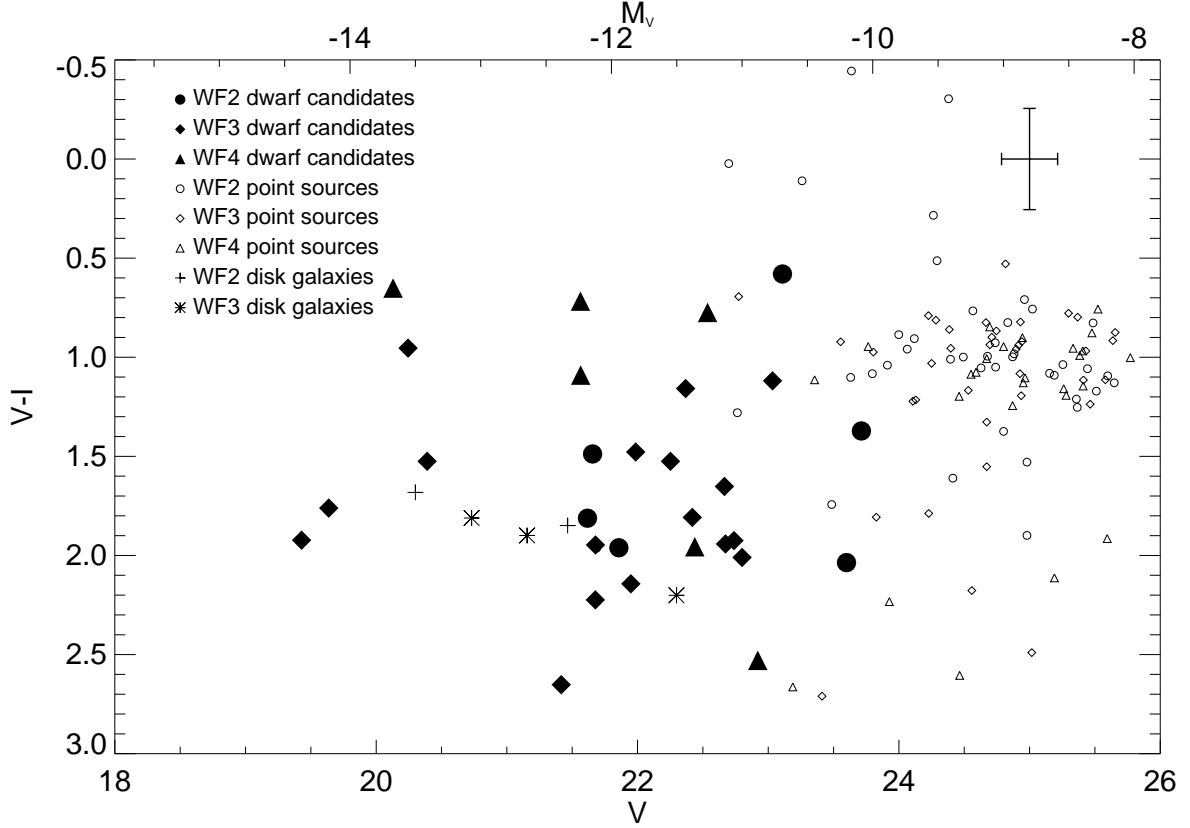


Fig. 10.— Color-magnitude diagram for extended sources detected in V (F555W) and I (F814W). The filled symbols represent extended sources on WF2 (filled circles), WF3 (filled diamonds), and WF4 (filled triangles). For reference, the point sources from Figure 5 are included as open polygons. The error bars in the upper right represent the mean error in the photometry of all extended objects. All of the photometry has been corrected for Galactic reddening. The absolute magnitude scale (top) is given for the objects at the distance of the Sextet, $57.5 h_{75}^{-1}$ Mpc.

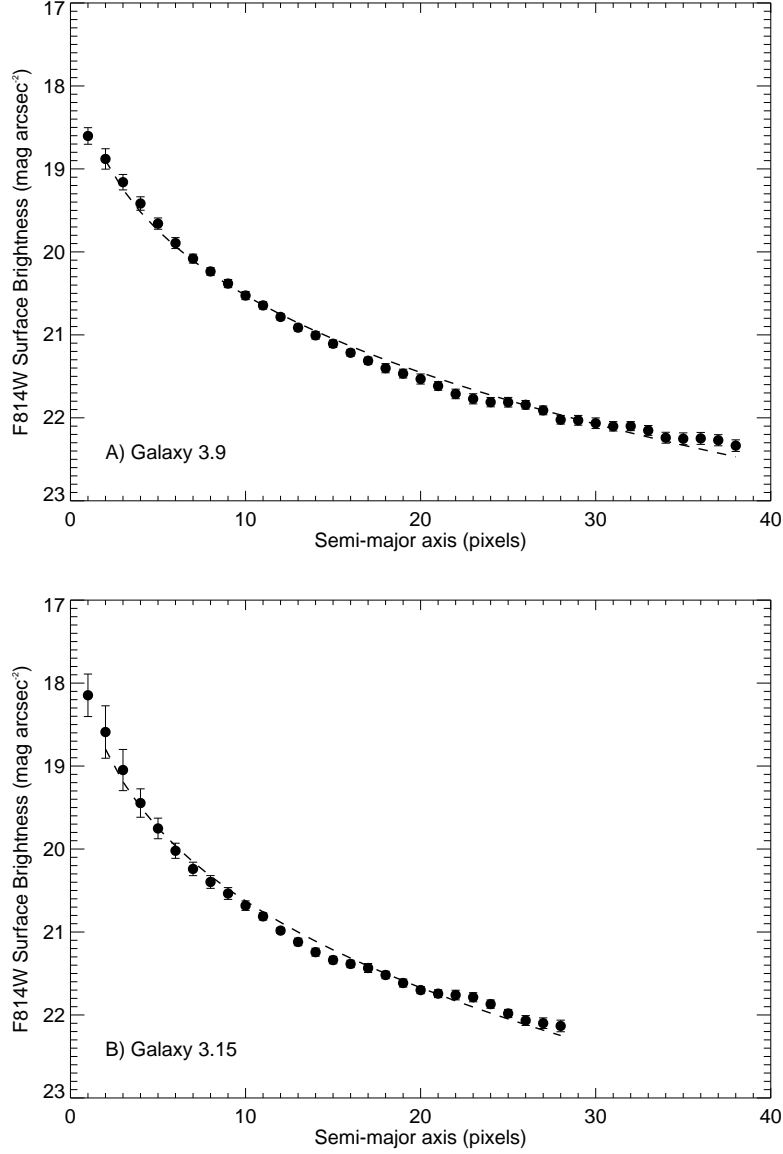


Fig. 11.— F814W surface brightness profiles for galaxies 3.9 (top panel) and 3.15 (bottom panel). Overplotted on the data are fits to a modified Sérsic profile with shape parameter $n = 1/4$, which is equivalent to the de Vaucouleurs $r^{1/4}$ law. Both objects are fit well with this type of profile and have central surface brightnesses of 15.6 (galaxy 3.9) and 15.1 (galaxy 3.15) mag arcsec⁻². The shapes of the profiles and the central surface brightnesses are consistent with those of giant elliptical galaxies.

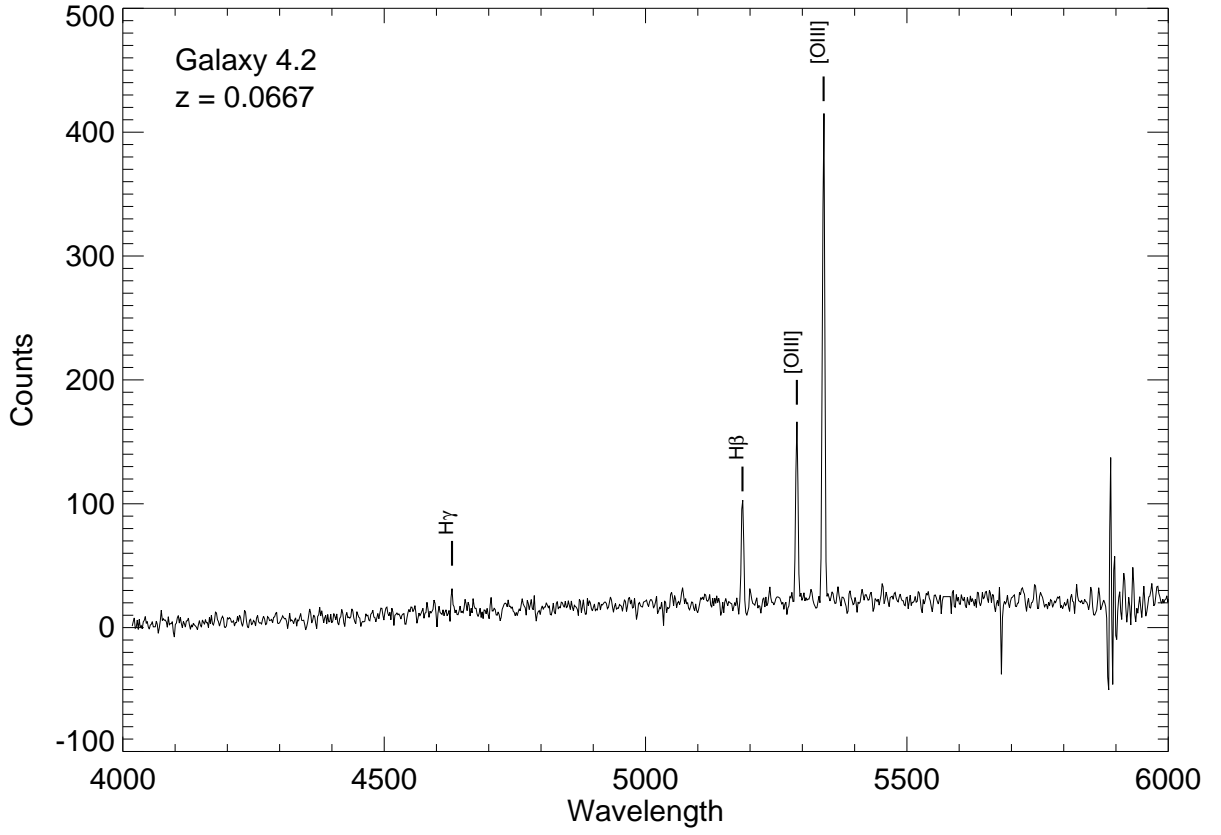


Fig. 12.— Hobby-Eberly Telescope spectrum of galaxy 4.2. Four emission lines are labeled, $H\gamma$, $H\beta$, and the O III $\lambda\lambda$ 4959, 5007 doublet. The redshift for this galaxy is $z = 0.0667$, which is nearly identical to that of the discordant spiral galaxy found in Seyfert’s Sextet, NGC6027e.

Table 1. Properties of Seyfert’s Sextet

Property ^a			
Alternate Names:	HCG 79, VV115, NGC6027		
Equatorial Coordinates:	15 ^h 59 ^m 12 ^s +20°45′31″ (J2000.0)		
Mean Redshift:	0.0145		
Radial Velocity Dispersion:	138 km s ^{−1}		
Galaxies:	Name	Type	v (km s ^{−1})
	NGC6027a	E0	4294
	NGC6027b	S0	4446
	NGC6027c	S0	4146
	NGC6027d	Sdm	4503
	NGC6027e	Scd	19809

^aData taken from Hickson (1994).

Table 2. Aperture Corrections

Filter	N_{stars}	Value	σ
F814W	17	−0.199	0.022
F555W	8	−0.149	0.033
F439W	6	−0.163	0.025
F336W	6	−0.144	0.021

Table 3. Photometric results for dwarf galaxy candidates

ID	F814W ^a	F555W ^a	F439W	F336W
2.6 ^b	22.63±0.25	23.28±0.19	~ 25.2	~ 24.0
3.3 ^c	20.83±0.11	22.42±0.19
3.8	22.02±0.20	23.20±0.25
3.10	21.31±0.18	22.54±0.23
3.14	19.39±0.06	20.42±0.06	21.39±0.28	21.70±0.59
4.1 ^b	21.86±0.22	22.71±0.20	~ 24.6	~ 23.4
4.2	19.58±0.15	20.30±0.13	21.37±0.22	20.98±0.42
4.3	20.95±0.12	21.73±0.13	23.01±0.27	22.21±0.35
4.6	20.58±0.12	21.74±0.15

^aThe magnitudes listed here have not been corrected for Galactic extinction. The values adopted for the extinction/reddening corrections are given in §2.3.

^bFor these two cases, the objects were detected in the two blue filters, but at low signal to noise. Rough limits to the magnitudes are provided, but the errors are likely to be > 0.5 magnitudes.

^cThis object is one of the “faint, red” galaxies on WF3, but it is included here due to its peculiar morphology and presence in the tidal debris of NGC6027c. The photometry presented here only represents the “head” of the galaxy and does not include the “tail” of emission that appears to be associated with this object.

Table 4. Emission Lines Detected in Spectrum of Galaxy 4.2

Line	λ_{obs} (Å)	redshift (km s ⁻¹) ^a
H γ	4629.5	19,960
H β	5185.4	19,987
[O III] λ 4959	5289.5	19,984
[O III] λ 5007	5340.7	19,988

^aFor consistency with the heliocentric velocities of HCG galaxies reported in Hickson et al. (1992), the redshift values listed here were calculated as $v = cz$.